Image Classification Algorithm for Graphite Ore Carbon Grade Based on Multi-scale Feature Fusion

Xueyu Huang[1,2], Haoyu Shi[1(✉)], Yaokun Liu[1], and Haoran Lu[1]

[1] School of Software Engineering, Jiangxi University of Science and Technology, Nanchang 330013, China
qq437211826@163.com

[2] Key Laboratory of Virtual Digital Factory and Cultural Communication, Jiangxi University of Science and Technology, Nanchang 330013, China

Abstract. Based on the tedious process of using a carbon-sulfur analyzer to detect the carbon grade of graphite in graphite mining production, this paper proposes a graphite carbon grade image recognition and classification method based on multi-scale feature fusion. The experiment preprocesses the images and constructs a residual network model that combines pyramid convolution (PyConv) and spatial attention mechanism (SAM). This model enhances the extraction of both global and local feature information from graphite images. Transfer learning is introduced by using pre-trained weights to accelerate the convergence of the model, achieving efficient and accurate recognition and classification of graphite carbon grade with an accuracy of 92.5%, surpassing traditional machine learning methods using single features. The experimental results demonstrate that the neural network model constructed in this paper effectively extracts texture and color features from graphite images, improving the accuracy of graphite image classification and recognition. The model exhibits good robustness and provides valuable insights for practical graphite mining production.

Keywords: Pyramid Convolution · Residual Network · Graphite Ore Carbon Grade · Image Classification · Attention Mechanism

1 Introduction

With the development of the new energy field, graphite has a wide range of applications as a negative electrode in the new energy industry. In the process of graphite mining and production, timely prediction of the carbon grade of graphite ore is particularly important. Traditionally, high-frequency infrared carbon-sulfur analyzers have been used for carbon grade determination in graphite mining [1, 2]. However, this method requires manual labor, time, and incurs costs such as machine wear and tear. With the advancement of industrial intelligence, mining production methods are gradually becoming more intelligent [3]. Therefore, proposing an efficient and convenient method for carbon grade detection in graphite mining is of significant practical importance.

C. Wu et al. (Eds.): MONAMI 2023, LNICST 559, pp. 166–177, 2024.
https://doi.org/10.1007/978-3-031-55471-1_13

Image recognition technology is one of the key areas in artificial intelligence. It aims to enable machines to mimic human image recognition systems and achieve recognition of complex images through processing information at different levels of the image. In traditional image recognition, the focus is on extracting features such as shape, texture, and color from the images [4–6]. Classification is typically performed using methods such as Support Vector Machine (SVM) [7], Random Forest (RF) [8], K-Nearest Neighbor (KNN) [9], and Back Propagation Neural Network (BPNN) [10]. However, traditional image recognition methods rely on manually extracting features and are limited in their ability to extract higher-dimensional features.

In recent years, with the continuous development of deep learning, its application in the field of image recognition has become increasingly widespread. Deep learning models, through multi-layer convolutional neural network structures, autonomously learn and extract more representative features [11, 12]. This enables various applications such as image recognition and classification, and has found extensive use in industrial domains. Chen Weihao et al. [13] proposed a deep residual neural network (ResNet) model that incorporates transfer learning methods for automatic classification of seven types of rock images. Cheng Guojian et al. [14] presented a deep learning-based automatic classification method for rock particle sizes using convolutional neural networks. Bai Lin et al. [15] utilized deep learning methods for rock identification and successfully extracted minerals from various types of rocks, demonstrating the effectiveness of deep learning in rock recognition. Bai Lin and Wei Xin [16] attempted to apply deep learning methods to thin section image classification and developed a VGG model for thin section classification of rocks. Liu Xiaobo et al. [17] employed a simplified VGG16 as the base feature extraction network within the Faster R-CNN deep learning object detection framework, creating a model for recognizing rock image categories.

Deep learning has achieved significant progress and development in the field of rock image recognition. However, most experiments have focused on distinguishing different types of rocks, while there has been limited research on identifying the content of a specific substance within the same type of rock.

To address the aforementioned situation and problem, this paper proposes an image recognition and classification method for graphite ore carbon grade based on multi-scale feature fusion. In the feature extraction stage of this approach, a pyramid structure neural network is employed, which consists of filters with different types, sizes, and depths, as well as grouped convolutions. This network extracts texture features and color features at different levels of the image. Furthermore, a spatial attention mechanism is introduced to localize the regions of interest, reducing the receptive field and improving context modeling. The extracted feature information is then fused. The fused features comprehensively capture the texture and color information of graphite ore images from multiple scales and levels. This enables more accurate identification and classification of graphite ore carbon grade.

The main contributions of this paper are as follows:

1) In the process of graphite ore image classification, the introduction of transfer learning allows for the full utilization of the generic features learned by a pre-trained model on a large-scale dataset. By fine-tuning the model for the specific task of graphite

ore image classification, the performance and generalization ability of the model are significantly improved, accelerating the training process.
2) To address the challenges of diverse textures and complex feature extraction in graphite ore images, a residual network based on pyramid convolution is utilized. By stacking convolutions with different sizes, this network can effectively capture multi-scale features.
3) To capture the differences and importance among different regions in graphite ore images, a spatial attention mechanism is incorporated. This mechanism automatically learns the significance of different regions and focuses on the most informative areas, enabling more accurate feature extraction, improving classification performance, and enhancing the robustness of the model.

In Sect. 2, the structure and details of the multi-scale feature fusion method for graphite ore carbon grade image classification are presented. Section 3 discusses the experimental setup, result analysis, and method comparisons. Finally, Sect. 4 concludes the paper.

2 Multi-scale Feature Fusion Method for Graphite Ore Carbon Grade Image Classification

This paper proposes a multi-scale feature fusion method for graphite ore carbon grade image classification, as illustrated in Fig. 1. Firstly, the graphite ore images are preprocessed. Secondly, the pyramid convolutional network, combined with the spatial attention mechanism, extracts multi-dimensional features from the preprocessed images and integrates them. Lastly, the features from different levels are fused, and the classification is performed using a classifier, resulting in a robust and high-accuracy model. This approach achieves the classification and recognition of various grades of graphite ore.

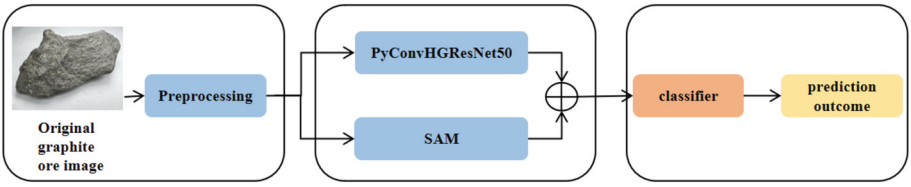

Fig. 1. Flowchart of the Proposed Method

2.1 Experimental Raw Data

Currently, there is a scarcity of publicly available graphite ore image datasets. The image data used in this experiment were collected from graphite mines by experienced professionals. The data were captured and annotated by professional personnel and equipment. To increase the size of the experimental dataset, multiple angles of the same

sample were photographed to capture different regions. The accurate carbon grade data for each sample was determined using a conventional carbon-sulfur analyzer, which was then matched with the corresponding images to create the final graphite ore carbon grade dataset. The overall carbon grade of the image dataset ranges from 0% to 20% and can be categorized into four classes: low-grade graphite ore (0% to 5%), relatively low-grade graphite ore (5% to 10%), relatively high-grade graphite ore (10% to 15%), and high-grade graphite ore (15% to 20%). Some original images from the experiment are shown in Fig. 2.

Fig. 2. Examples of Graphite Ore Samples with Different Carbon Grades

Each image has a resolution of 6000x4000 pixels, and a total of 8159 images were used in this study. All images are in.JPG format. The dataset was randomly divided into training and testing sets in an 8:2 ratio for each class of images. The training set consists of 6529 images, while the testing set consists of 1630 images. The distribution of the graphite ore image dataset for each class is shown in Table 1.

Table 1. Distribution of Graphite Ore Image Dataset

Dataset Type	Different Carbon Grade Graphite Ores				Total Count
	0%–5%	5% ~ 10%	10%–15%	15%–20%	
Total Count	1207	1729	3286	1937	8159
Training Set	966	1383	2629	1550	6529
Testing Set	241	346	657	387	1630

2.2 Graphite Ore Image Feature Extraction

Multi-scale Feature Extraction Based on Pyramid Convolution

Pyramid Convolution Structure (PyConv)

Graphite ore surfaces exhibit high complexity in terms of texture features, and the diverse texture distribution resulting from multi-angle image acquisition further increases the complexity. To capture the variability of different categories and their scale variations, using a single type of convolutional kernel (e.g., standard convolution) and a single spatial size may not be the optimal solution for addressing this complexity. Therefore, the conventional convolutional neural networks (e.g., ResNet50) for image feature extraction have limitations.

The pyramid convolution structure consists of convolutional kernels of different levels, sizes, and depths. In addition to enlarging the receptive field, PyConv can process inputs in parallel using different-sized convolutional kernels to capture details at different levels. Apart from these advantages, after designing its structure, PyConv can maintain a similar number of parameters and computational costs as standard convolution. Therefore, we adopt pyramid convolution to replace traditional convolution and construct a pyramid convolutional neural network.

The pyramid convolution, as shown in Fig. 3, consists of n layers of convolutional kernels with different types, without increasing computational cost or model complexity. At each level of PyConv, the spatial size of the convolutional kernels varies, starting from the bottom of the pyramid (Level 1 of PyConv) and gradually increasing towards the top (Level n of PyConv). Simultaneously, as the spatial size increases, the depth of the convolutional kernels decreases from Level 1 to Level n. At each level of PyConv, convolutional kernels of different depths are used, and the input feature maps are divided into different groups. The convolutional kernels are independently applied to each group of input feature maps, which is known as grouped convolution.

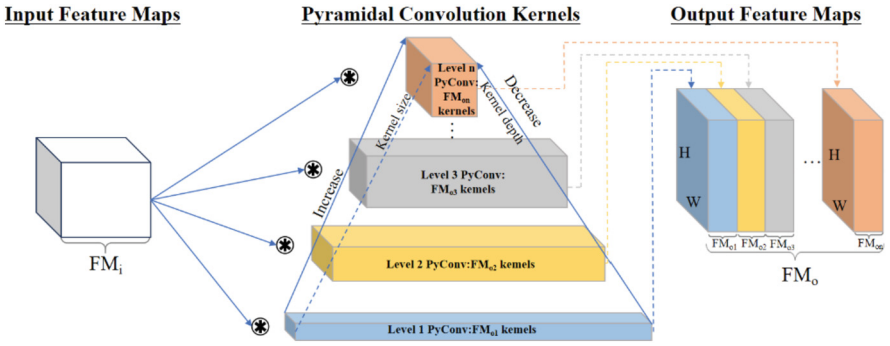

Fig. 3. Proposed Pyramidal Convolution Structure Model

As shown in Fig. 3, for the input feature map FM_i, at each level {1, 2, 3, . . . , n} of PyConv, different convolutional kernels $\{K_1^2, K_2^2, K_3^2, \ldots, K_n^2\}$ with different spatial sizes and different convolutional kernel depths $\{FM_i, \frac{FM_i}{\left(\frac{K_2^2}{K_1^2}\right)}, \frac{FM_i}{\left(\frac{K_3^2}{K_1^2}\right)}, \ldots, \frac{FM_i}{\left(\frac{K_n^2}{K_1^2}\right)}\}$ are applied. This results in different numbers of output feature maps $\{FM_{o1}, FM_{o2}, FM_{o3}, \ldots, FM_{on}\}$ (with height H and width W). Therefore, the number of parameters and computational cost (in terms of FLOPs) of PyConv are given by:

$$\left| \begin{array}{l} parameters = \\ K_n^2 \cdot \frac{FM_i}{\left(\frac{K_n^2}{K_1^2}\right)} \cdot FM_{o_n} + \\ \vdots \\ K_2^2 \cdot \frac{FM_i}{\left(\frac{K_2^2}{K_1^2}\right)} \cdot FM_{o_2} + \\ K_1^2 \cdot FM_i \cdot FM_{o_1}; \end{array} \right| \left| \begin{array}{l} FLOPs = \\ K_n^2 \cdot \frac{FM_i}{\left(\frac{K_n^2}{K_1^2}\right)} \cdot FM_{o_n} \cdot (W \cdot H) + \\ \vdots \\ K_2^2 \cdot \frac{FM_i}{\left(\frac{K_2^2}{K_1^2}\right)} \cdot FM_{o_2} \cdot (W \cdot H) + \\ K_1^2 \cdot FM_i \cdot FM_{o_1} \cdot (W \cdot H), \end{array} \right| \quad (1)$$

In the Eq. (1), each row represents the parameter count and computational cost of one level of PyConv. If each level of PyConv outputs an equal number of feature maps, then the parameter count and computational cost of PyConv will be evenly distributed across each level of the pyramid. From the equation, it can be observed that regardless of the number of levels in PyConv and the spatial size of the convolutional kernels, its computational cost and parameter count are similar to that of a standard convolution with a single kernel size $K_1{}^2$.

Pyramid Residual Network Structure

Based on the ResNet residual module, the pyramid convolution is incorporated.Table 2 presents a comparison between PyConvResNet and the baseline architecture ResNet, showcasing a 50-layer deep network scenario. It also demonstrates a higher group number architecture of PyConv, called PyConvHGResNet, where the group number is set to a minimum of 32 and a maximum of 64. The feature map quantity for spatial convolution is doubled to provide better spatial filtering capability, which slightly increases the number of FLOPs.

Table 2. Comparison of PyConvResNet and PyConvHGResNet

Stage	output	ResNet-50	PyConvResNet-50	PyConvHGResNet-50
	112 × 112	7 × 7,64, stride 2	7 × 7,64,stride 2	7 × 7,64,stride 2
		3 × 3max pool, stride 2		

(*continued*)

Table 2. (*continued*)

Stage	output	ResNet-50	PyConvResNet-50	PyConvHGResNet-50
Stage1	56 × 56	$\begin{bmatrix} 1\times1, 64 \\ 3\times3, 64 \\ 1\times1, 256 \end{bmatrix} \times 3$	$\begin{bmatrix} 1\times1, 64 \\ \text{PyConv4, 64 :} \\ \begin{bmatrix} 9\times9, 16, G=16 \\ 7\times7, 16, G=8 \\ 5\times5, 16, G=4 \\ 3\times3, 16, G=1 \end{bmatrix} \\ 1\times1, 256 \end{bmatrix} \times 3$	$\begin{bmatrix} 1\times1, 128 \\ \text{PyConv4, 128 :} \\ \begin{bmatrix} 9\times9, 32, G=32 \\ 7\times7, 32, G=32 \\ 5\times5, 32, G=32 \\ 3\times3, 32, G=32 \end{bmatrix} \\ 1\times1, 256 \end{bmatrix} \times 3$
Stage2	28 × 28	$\begin{bmatrix} 1\times1, 128 \\ 3\times3, 128 \\ 1\times1, 512 \end{bmatrix} \times 4$	$\begin{bmatrix} 1\times1, 128 \\ \text{PyConv3, 128 :} \\ \begin{bmatrix} 7\times7, 64, G=8 \\ 5\times5, 32, G=4 \\ 3\times3, 32, G=1 \end{bmatrix} \\ 1\times1, 512 \end{bmatrix} \times 4$	$\begin{bmatrix} 1\times1, 256 \\ \text{PyConv3, 256 :} \\ \begin{bmatrix} 7\times7, 128, G=64 \\ 5\times5, 64, G=64 \\ 3\times3, 64, G=32 \end{bmatrix} \\ 1\times1, 512 \end{bmatrix} \times 4$
Stage3	14 × 14	$\begin{bmatrix} 1\times1, 256 \\ 3\times3, 256 \\ 1\times1, 1024 \end{bmatrix} \times 6$	$\begin{bmatrix} 1\times1, 256 \\ \text{PyConv2, 256 :} \\ \begin{bmatrix} 5\times5, 128, G=4 \\ 3\times3, 128, G=1 \end{bmatrix} \\ 1\times1, 1024 \end{bmatrix} \times 6$	$\begin{bmatrix} 1\times1, 512 \\ \text{PyConv2, 512 :} \\ \begin{bmatrix} 5\times5, 256, G=64 \\ 3\times3, 256, G=32 \end{bmatrix} \\ 1\times1, 1024 \end{bmatrix} \times 6$
Stage4	7 × 7	$\begin{bmatrix} 1\times1, 512 \\ 3\times3, 512 \\ 1\times1, 2048 \end{bmatrix} \times 3$	$\begin{bmatrix} 1\times1, 512 \\ \text{PyConv1, 512 :} \\ [3\times3, 512, G=1] \\ 1\times1, 2048 \end{bmatrix} \times 3$	$\begin{bmatrix} 1\times1, 1024 \\ \text{PyConv1, 1024 :} \\ [3\times3, 1024, G=32] \\ 1\times1, 2048 \end{bmatrix} \times 3$
	1 × 1	global avg pool 1000-d fc	global avg pool 1000-d fc	global avg pool 1000-d fc
FLOPs		4.14×10^9	3.88×10^9	4.61×10^9
#params		25.56×10^6	24.85×10^6	25.23×10^6

Spatial Attention Mechanism (SAM)

Introducing the spatial attention mechanism into the model enables adaptive allocation of attention weights, focusing on the most informative and important regions in the image. This enhances the model's ability to capture and understand key features, improving the accuracy and robustness of image processing tasks. In this study, the spatial attention module is placed before the first residual structure and after the last residual structure. Figure 4 illustrates the structure of the spatial attention mechanism.

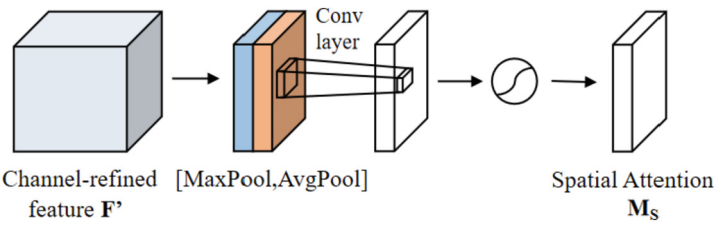

Fig. 4. Spatial Attention Module

3 Experimental Results and Analysis

3.1 Experimental Setup

The hardware environment for this study consisted of the following specifications: operating system: Windows 10, GPU: Nvidia GeForce RTX 3080 (10 GB), CPU: 12-core Intel(R) Xeon(R) Platinum 8255C CPU @ 2.50 GHz. The software environment included PyTorch 1.9.0, Python 3.8, and CUDA 11.3.

3.2 Network Model Ablation Experiments

In this study, a series of ablation experiments were conducted on a professionally collected graphite ore image dataset to verify the effectiveness of various improvement modules in the task of graphite ore image classification. The purpose was to gain a deeper understanding of the impact of different modules on graphite ore image classification and their role in the overall network performance. The specific combinations are described as follows (as shown in Table 3):

Baseline: The Baseline model is a conventional ResNet50 residual network model.

Baseline + PyConv: This combination replaces the 3 × 3 convolutional layers in the ResNet50 residual structure with Pyramid Convolution (PyConv). By using convolutional kernels of different sizes and depths, it extracts more multidimensional feature information from graphite ore images, captures spatial context dependencies, and improves model performance.

Baseline + PyConv + HG: This combination builds upon Baseline + PyConv by using a higher number of groups, doubling the spatial convolution feature quantity. This enhances spatial filtering capability and improves feature extraction, thereby enhancing the network's ability to represent and express input data.

Baseline + PyConv + HG + SAM: This combination incorporates the Spatial Attention Mechanism (SAM) into the entire residual structure network before and after Baseline + PyConv + HG. By adaptively allocating attention weights, it improves the model's ability to capture key features in graphite ore images, thereby enhancing the accuracy and robustness of image classification.

Table 3. Comparative Analysis of Ablation Experiments for Different Module Combinations.

Model Variants	Modules			Accuracy (%)
	PyConv	HG	SAM	
Baseline				90.2%
Baseline + PyConv	√			91.5%
Baseline + PyConv + HG	√	√		92.2%
Baseline + PyConv + HG + SAM	√	√	√	92.5%

3.3 Comparative Experiments with Other Methods

This section compares the performance of the PyConvHGResNet50-SAM, a pyramid convolutional neural network, with other popular convolutional neural networks in the field of graphite mineral image classification. The comparison includes the ResNet series of residual networks, specifically ResNet50 and ResNet101, the lightweight neural network MobileNet series, specifically MobileNet_V2, the dense convolutional network DenseNet series, specifically DenseNet121, and the PyConvResNet101, which is based on the deeper pyramid convolutional layers proposed in this paper.

In the training process of each model, the same parameter settings were selected to ensure a fair and objective comparison between different models. The image resolution was uniformly adjusted to 224 × 224 before inputting into the network. The batch size was set to 32, meaning that 32 images were selected for training in each iteration. The maximum number of training epochs was set to 400. The SGD optimizer was used to update the model parameters, with an initial learning rate of 0.01, a decay parameter of 0.005, and a momentum parameter of 0.9. The training was stopped when the model converged. Figure 5 shows the accuracy of the six models on the test set as a function of the number of training epochs, and Fig. 6 shows the corresponding loss values as a function of the number of epochs.

From Fig. 5, it can be observed that, under the same batch size, all models benefit from the introduction of transfer learning and the use of pre-trained weights, resulting in a rapid improvement in accuracy during the initial stages of training. The DenseNet121 model reaches an accuracy of 80% after 50 epochs and shows a slow but steady increase. It converges at around 350 epochs with accuracy fluctuating around 87%. The MobileNet_V2 model reaches 78% accuracy after 50 epochs but experiences more significant fluctuations during the training process. It converges at around 330 epochs with accuracy fluctuating around 87%. The ResNet50 model, based on the conventional residual network, converges after approximately 300 epochs with accuracy fluctuating around 89%. The ResNet101 model also converges after 300 epochs with accuracy fluctuating around 88%. The PyConvResNet101 model, with its higher depth and multi-size convolutional kernels, starts to converge at around 270 epochs with accuracy fluctuating around 89%. On the other hand, the PyConvHGResNet50-SAM model reaches its highest accuracy of 85% relative to other models after approximately 50 epochs, and then converges at around 300 epochs with accuracy fluctuating around 91%.

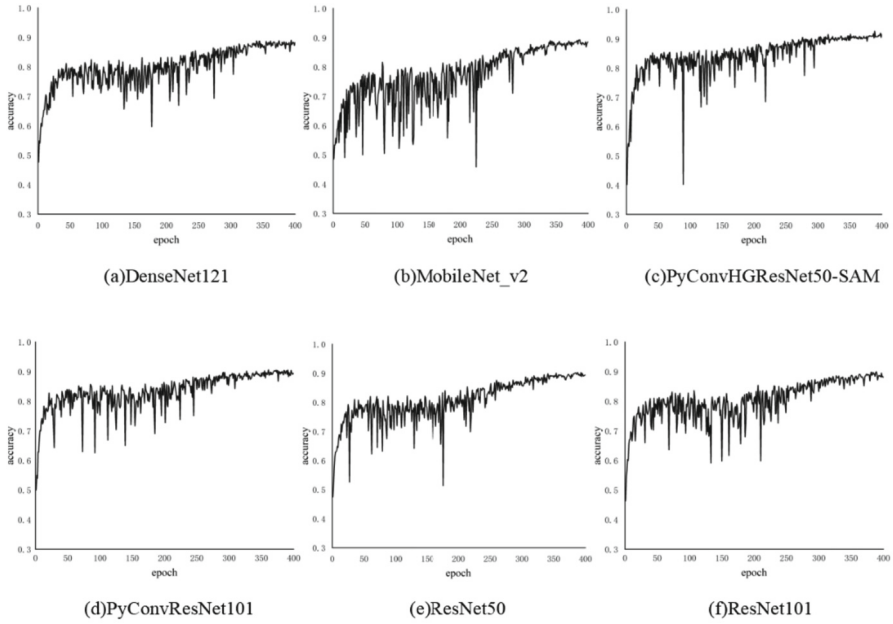

Fig. 5. Compares the accuracy of the six neural network models.

According to the comparison of loss values in Fig. 6, the DenseNet121 model shows a rapid decrease in loss to around 0.28 after 50 epochs, and it converges around 350 epochs with fluctuations around 0.07. The MobileNet_V2 model exhibits a similar trend, with the loss dropping to 0.37 after 50 epochs and converging around 0.08 after 350 epochs. The loss curves of ResNet50 and ResNet101 are similar, converging around 360 epochs with fluctuations around 0.055. Both the PyConvResNet101 and PyConvHGResNet50-SAM models show similar patterns, with the loss decreasing to below 0.2 after 50 epochs and converging around 0.045 after 350 epochs. Considering both accuracy and loss, it can be concluded that the PyConvHGResNet50-SAM model achieves the highest accuracy while maintaining a fast convergence speed, making it the most effective among the compared models.

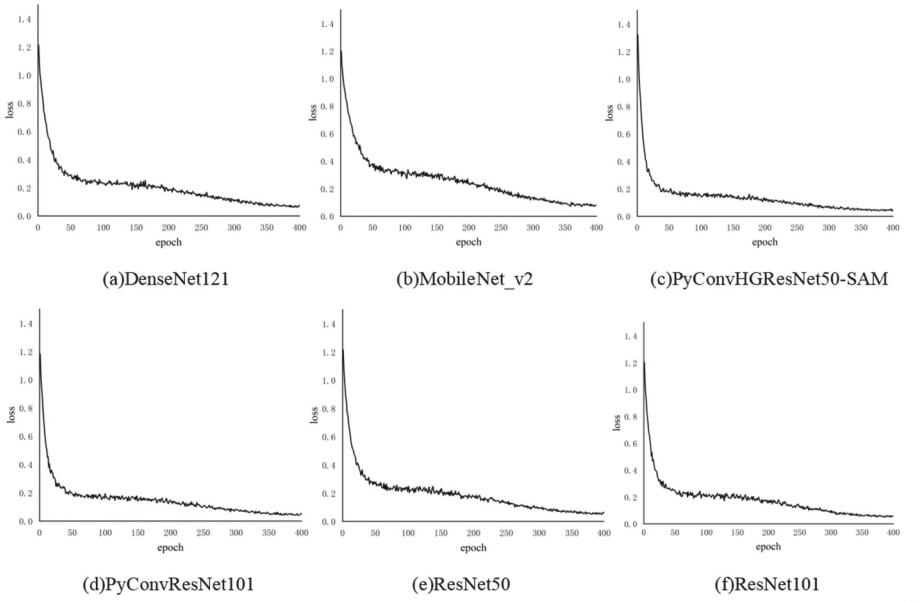

Fig. 6. Comparison of Loss Values for Six Neural Networks

4 Conclusion

In this study, we proposed a method for graphite ore carbon grade image classification based on multi-scale feature fusion. We replaced the convolutional layers in the traditional residual structure with a newly designed pyramid convolutional layer, which consists of convolutional kernels with different sizes and depths. This enables the extraction of complex texture features from multiple dimensions on the surface of graphite ore. We introduced transfer learning to accelerate model convergence and incorporated spatial attention mechanism to focus on important information in the regions of interest, thus improving the accuracy of the model. Experimental results demonstrated that our method outperforms other existing methods in terms of classification accuracy. Moreover, compared to traditional carbon-sulfur analyzers used for detecting graphite ore carbon grade, our method offers advantages such as higher efficiency, accuracy, and convenience. It is feasible and of significant importance for the construction of smart mines.

References

1. Xie, J.: Exploration of the method for determining the fixed carbon content in carbonate graphite ore based on high-frequency infrared. Gansu Sci. Technol. **39**(01), 18–20 (2023)
2. Liu, Y., Xiang, L., Dong, A., et al.: Study on the method of measuring fixed carbon in graphite by high-frequency infrared carbon-sulfur analyzer. Chem. Eng. Des. Commun. **47**(11), 44–45 (2021)

3. Chai, F.: Exploration and practice of intelligent mine construction in Zhengzhuang coal mine. Shandong Coal Sci. Technol. **40**(12), 25–27+34 (2022)
4. Pinto, D.L., et al. Image feature extraction via local binary patterns for marbling score classification in beef cattle using tree-based algorithms. Livestock Sci. 267 (2023)
5. Baigts, A.D., Ramírez, RM., Rosas, R.R.: Monitoring of the dehydration process of apple snacks with visual feature extraction and image processing techniques. Appl. Sci. **12**(21), 11269–11269 (2022)
6. Singh, N., Singh, T.N., Tiwary, A., Sarkar, K.: Textural identification of basaltic rock mass using image processing and neural network. Comput. Geosci. **14**, 301–310 (2010)
7. Deepa, S., Umarani, R.: Steganalysis on images using SVM with selected hybrid features of Gini index feature selection algorithm. Int. J. Adv. Res. Comput. Sci. **8**(5), 1503–1509 (2017)
8. Yang, L., Bai, Z., Kou, Y.G.: Analysis of the loss of civil aviation customers by random forest algorithm based on RFM model. Comput. Modernization **1**, 100–104 (2021)
9. Guettari, N., Capelle-Laizé, A.S., Carr, P.: Blind image steganalysis based on evidential K-Nearest neighbors. In: Proceedings of the 2016 IEEE International Conference on Image Processing, 2742–2746 (2016)
10. Dong, W.K., Min, S.K., Lee, J., et al.: Adaptive learning rate backpropagation neural network algorithm based on the minimization of mean square deviation for impulsive noises. IEEE Access **8**, 98018–98026 (2020)
11. Zhou, N., Ouyang, X.Y.: Development of convolutional neural networks. J. Liaoning Univ. Sci. Technol. **44**(05), 349–356 (2021)
12. Yan, C., Wang, C.: Development and application of convolutional neural network models. J. Comput. Sci. Explor. **15**(01), 27–46 (2021)
13. Chen, W., et al.: Rock image classification using deep residual neural network with transfer learning. Front. Earth Sci. (2023)
14. Cheng, G., Guo, W., Fan, P.: Rock image classification based on convolutional neural network. J. Xi'an Shiyou Univ. (Nat. Sci. Edit.) **32**(04), 116–122 (2017)
15. Bai, L., Yao, Y., Li, S., Xu, D., Wei, X.: Mineral composition analysis of rock images based on deep learning feature extraction. China Min. **27**(07), 178–182 (2018)
16. Bai, L., Wei, X., Liu, Y., Wu, C., Chen, L.: Rock thin section image recognition based on VGG model. Geol. Bull. **38**(12), 2053–2058 (2019)
17. Liu, X., Wang, H., Wang, L.: Intelligent recognition of rock types based on Faster R-CNN method. Mod. Min. **35**(05), 60–64 (2019)